Supplementary Information

Synergistic carrier and phonon transport advance Ag dynamically-doped *n*-type PbTe thermoelectrics *via* Mn alloying

Wei Yuan, ‡[a] Qian Deng, ‡[a] Dong Pan, [b] Xiang An, [a] Canyang Zhao, [a] Wenjun Su, [a] Zhengmin He, [a] Qiang Sun*[c,d] and Ran Ang*[a,e]

[a] *Key Laboratory of Radiation Physics and Technology, Ministry of Education, Institute of Nuclear Science and Technology, Sichuan University, Chengdu 610064, China*

[b] *State Key Laboratory of Superlattices and Microstructures, Institute of Semiconductors, Chinese Academy of Sciences, P.O. Box 912, Beijing 100083, China*

[c] *State Key Laboratory of Oral Diseases, National Clinical Research Center for Oral Diseases, West China Hospital of Stomatology, Sichuan University, Chengdu, Sichuan 610041, China*

[d] *Sichuan Provincial Engineering Research Center of Oral Biomaterials, Chengdu, Sichuan 610041, China*

[e] *Institute of New Energy and Low-Carbon Technology, Sichuan University, Chengdu 610065, China*

‡ W. Yuan and Q. Deng contributed equally to this work.

*Corresponding authors and Emails: rang@scu.edu.cn (RA), qiangsun@scu.edu.cn (QS)

1. Computational details

1.1 Single parabolic band model

The Pisarenko curves and the effective mass of *n*-type PbTe can be modeled by the single parabolic band (SPB) model, and the SPB model is based on the following equations:[1]

Seebeck coefficient:

$$S = \pm\frac{k_B}{e}\left(\frac{(r+5/2)F_{r+2/3}(\eta)}{(r+3/2)F_{r+1/2}(\eta)}-\eta\right) \quad \text{(eq. S1)}$$

Hall carrier concentration:

$$n_H = 4\pi\left[\frac{2m^* k_B T}{h^2}\right]^{3/2}F_{1/2} \quad \text{(eq. S2)}$$

Lorenz number:

$$L = \frac{k_B^2 3F_0F_2 - 4F_1^2}{e^2 \quad F_0^2} \quad \text{(eq. S3)}$$

where k_B is the Boltzmann constant, $\hbar$ is the reduce Planck constant, η is the reduced Fermi level, and r denotes the scattering factor and equals -1/2 here assuming that the acoustic scattering mechanism dominates. The Fermi integral is given by:

$$F_n(\eta) = \int_0^\infty \frac{x^n}{1+e^{x-\eta}}dx \quad \text{(eq. S4)}$$

1.2 Single Kane band model

The thermoelectric-transport properties of *n*-type PbTe can be modeled by adopting the single Kane band (SKB) model. The transport coefficients are determined by the equations as follows:[2, 3]

Hall carrier concentration:

$$n_H = \frac{1}{eR_H} = A^{-1}\frac{N_V\left(2m_b^* k_B T\right)^{3/2}}{3\pi^2\hbar^3}{}^0F_0^{3/2} \quad \text{(eq. S5)}$$

Hall factor:

$$A = \frac{3K(K+2)\,{}^0F_{-4}^{1/2}\,{}^0F_0^{3/2}}{(2K+1)^2\quad\left({}^0F_{-2}^{1}\right)^2} \quad \text{(eq. S6)}$$

Hall Carrier mobility:

$$\mu_H = A\frac{2\pi\hbar^4 eC_l \qquad 3^0F_{-2}^{\ 1}}{m_I^*\left(2m_b^* k_B T\right)^{3/2} E_{def}^{\ 2}\ {}^0F_0^{3/2}} \qquad \text{(eq. S7)}$$

Power factor:

$$PF = \frac{2N_V\hbar {k_B}^2 C_l}{\pi E_{def}^{\ 2}}\frac{1}{m_I^*}\left(\frac{^1F_{-2}^{\ 1}}{^0F_{-2}^{\ 1}} - \xi\right)^2 {}^0F_{-2}^{\ 1} \qquad \text{(eq. S8)}$$

${}^nF_k^m$ has a similar form as the Fermi integral:

$${}^nF_k^m = \int_0^\infty \left(-\frac{\partial f}{\partial \varepsilon}\right)\varepsilon^n\left(\varepsilon + \alpha\varepsilon^2\right)^m\left[(1+2\alpha\varepsilon)^2 + 2\right]^{k/2} d\varepsilon \qquad \text{(eq. S9)}$$

Where ξ is the reduced chemical potential, N_v is the band degeneracy (N_V=4 for *n*-type PbTe),[4] *K* is the band anisotropy (*K*=3.6 for *n*-type PbTe),[5] k_B is the Boltzmann constant, $\hbar$ is the reduce Planck constant, m_I^* is the inertial mass ($m_I^* = 3m_d^*/(N_V^{2/3}(2K^{1/3} + K^{-2/3}))$),[6] C_l is the longitudinal elastic (C_l=7.1×1010 Pa for *n*-type PbTe),[7, 8] ε is the reduced energy of electronic state, α is the reciprocal reduced band gap ($\alpha = k_B T/E_g$), E_g is the band gap , $E_g = 0.18eV + 0.0004\ eV/K \times T$, E_{def} is the deformation potential coefficient.

1.3 Calculation of lattice thermal conductivity κ_{lat}

The lattice thermal conductivity (κ_{lat}) of the $Ag_{0.03}Pb_{1-x}Mn_xTe$ samples was calculated by the modified Debye-Callaway model, which can be expressed by:

$$\kappa_{lat} = \frac{k_B}{2\pi^2 v}\left(\frac{k_B}{\hbar}\right)^3 \int_0^{\Theta/T} \tau_{tot}(x)\frac{x^4 e^x}{\left(e^x - 1\right)^2} dx \qquad \text{(eq. S10)}$$

Here, $v = 3^{1/3}(v_l^{-3} + 2v_t^{-3})^{-1/3}$ is the average speed of phonon, v_l and v_t denote the longitudinal and transverse speeds of sound respectively, $\hbar$ is the reduced Planck constant, Θ is the Debye temperature, *x* is the relation of $\hbar\omega/k_B T$, ω is the phonon frequency, and τ_{tot} is the total phonon scattering relaxation time. The total phonon relaxation time τ_{tot} for the $Ag_{0.03}Pb_{1-x}Mn_xTe$ samples consists of Umklapp process, normal process, point defects, grain boundary, and nanoprecipitates (U+N+PD+GB+NP) by the following equation:[9]

$$\tau_{tot}^{-1} = \tau_U^{-1} + \tau_N^{-1} + \tau_{PD}^{-1} + \tau_{GB}^{-1} + \tau_{NP}^{-1} \qquad \text{(eq. S11)}$$

The phonon scattering relaxation time for respective mechanism can be expressed as follows:

Umklapp phonon scattering:

$$\tau_U^{-1} = A_N * \frac{2}{(6\pi^2)^{\frac{1}{3}}} \frac{k_B \bar{V}^{1/3} \omega^2 \gamma^2 T}{\bar{M} v^3} \quad \text{(eq. S12)}$$

Normal phonon scattering:

$$\tau_N^{-1} = \frac{2}{(6\pi^2)^{\frac{1}{3}}} \frac{K_B \bar{V}^{1/3} \omega^2 \gamma^2 T}{\bar{M} v^3} \quad \text{(eq. S13)}$$

Point defect scattering:

$$\tau_{PD}^{-1} = \frac{V\omega^4}{4\pi^3 v^3} * \sum (1-x_i)\left[\left(\frac{M_i - M}{M}\right)^2 + \varepsilon\left(\frac{a_i - a}{a}\right)^2\right] \quad \text{(eq. S14)}$$

Grain boundary scattering:

$$\tau_{GB}^{-1} = v/Gd \quad \text{(eq. S15)}$$

Nanoprecipitates scattering:

$$\tau_{NP}^{-1} = v[(2\pi R^2)^{-1} + (\frac{4}{9}\pi R^2 (\Delta D/D)^2 (\frac{\omega R}{v})^4)^{-1}]^{-1} N_p \quad \text{(eq. S16)}$$

In above equations, $\bar{V}$ is the average atomic volume, $\bar{M}$ is the average atomic mass, γ is the Grüneisen parameter, A_N is the ratio between normal process and Umklapp phonon scattering.

1.4 Calculation of quality factor *B*

The quality factor B of the $Ag_{0.03}Pb_{1-x}Mn_xTe$ samples was calculated by:[10]

$$B = \left(\frac{k_B}{e}\right)^2 \frac{8\pi e (2m_e k_B T)^{3/2} \mu_W}{3h^3 \quad \kappa_{lat}} T \quad \text{(eq. S17)}$$

2. Supplementary Figures

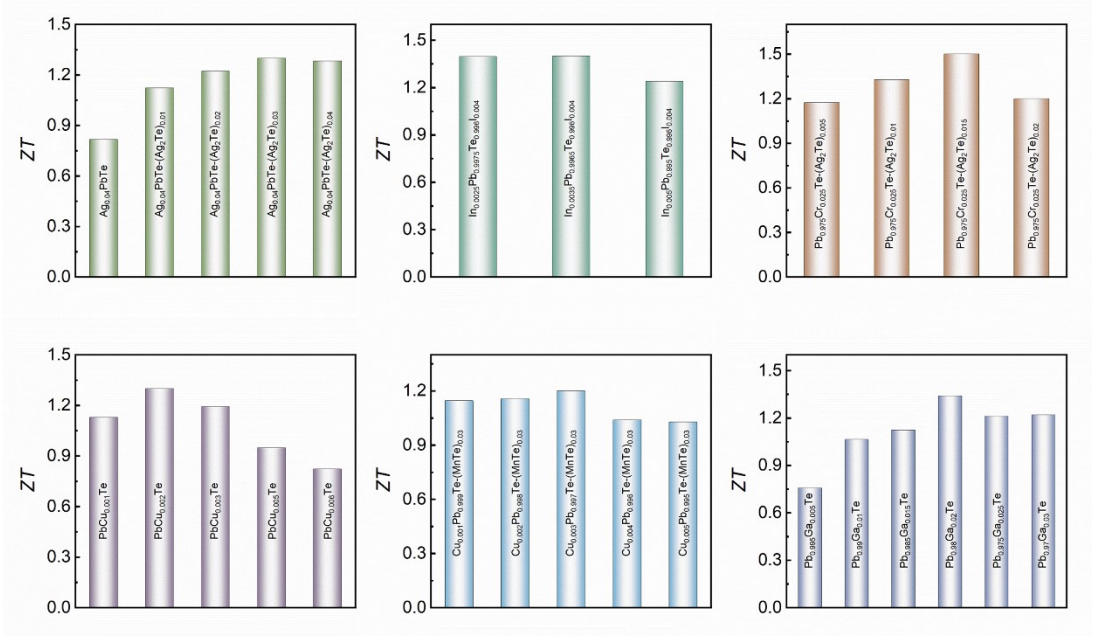

Figure S1. *ZT* of the main components of dynamic doped PbTe systems.[11-16]

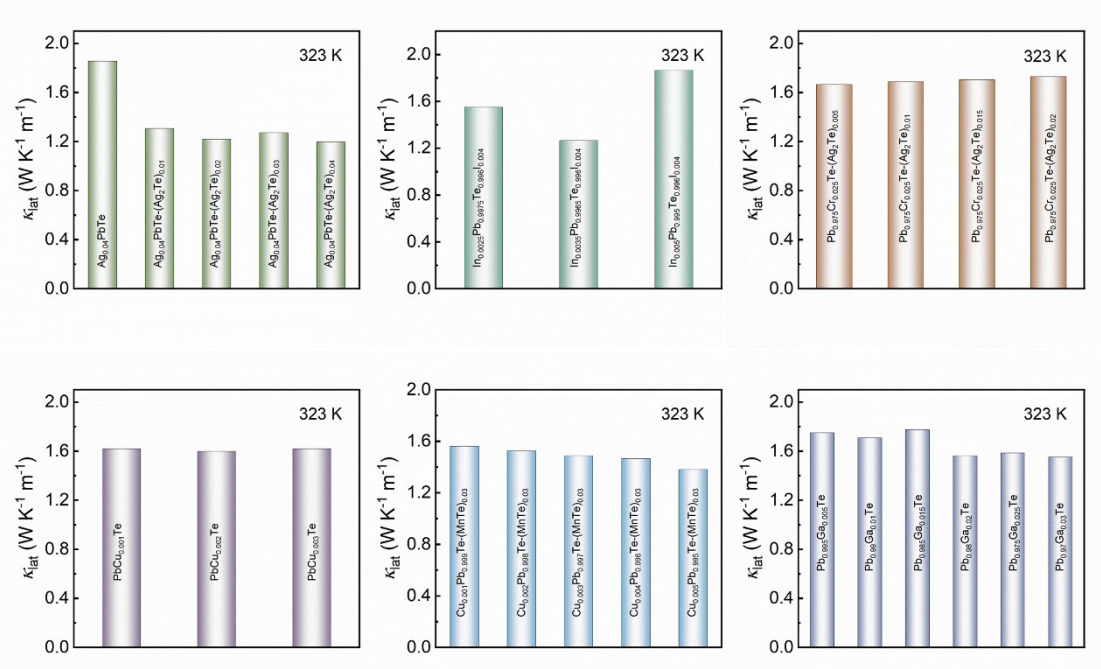

Figure S2. κ_{lat} at 323 K of the main components of dynamic doped PbTe systems.[11-16] the Lorenz number calculation methods for representative samples of each system: single parabolic band (SPB) model: PbTe:Cr/Ag2Te, PbTe:Ag, PbTe:Cu/MnTe, PbTe:Ga; single Kane band (SKB) model: PbTe:In/I, PbTe:Cu.

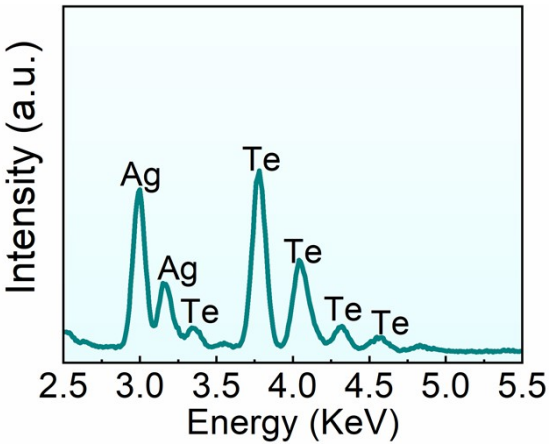

Figure S3. EDS spectra obtained from Ag_2Te secondary phase.

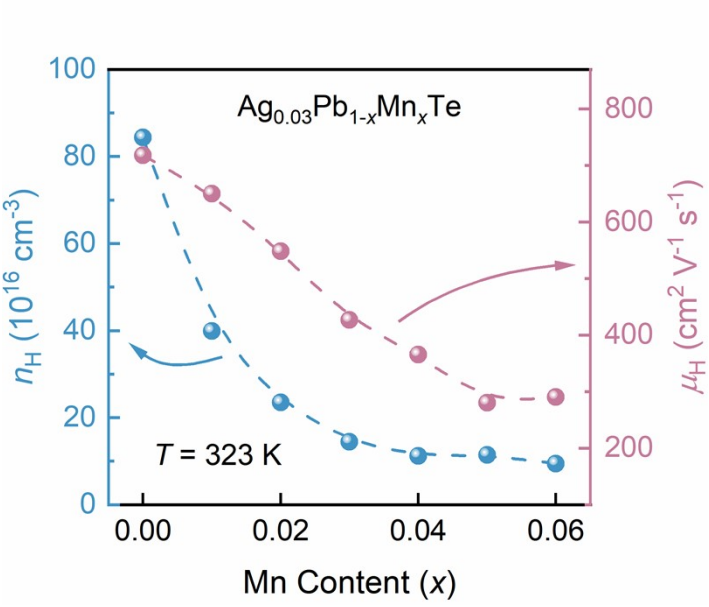

Figure S4. The Hall carrier concentration n_H and the Hall carrier mobility μ_H as a function of x in $Ag_{0.03}Pb_{1-x}Mn_xTe$.

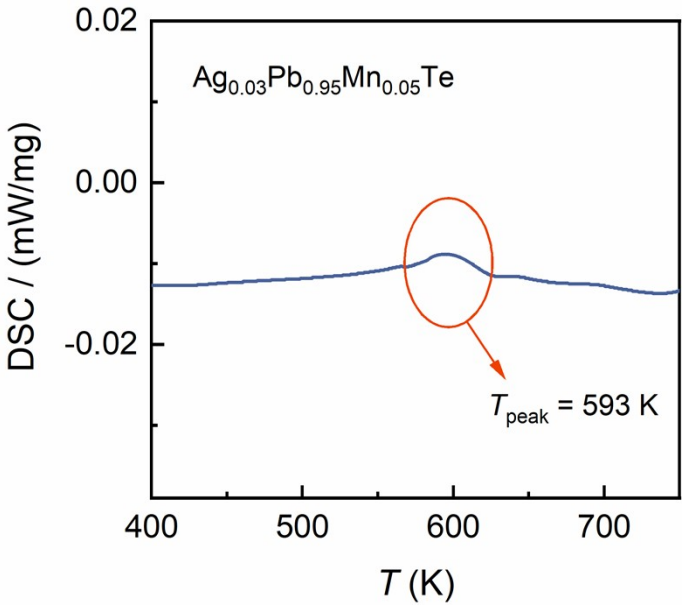

Figure S5. DSC curve of $Ag_{0.03}Pb_{0.95}Mn_{0.05}Te$, and the peak occurs at 593 K

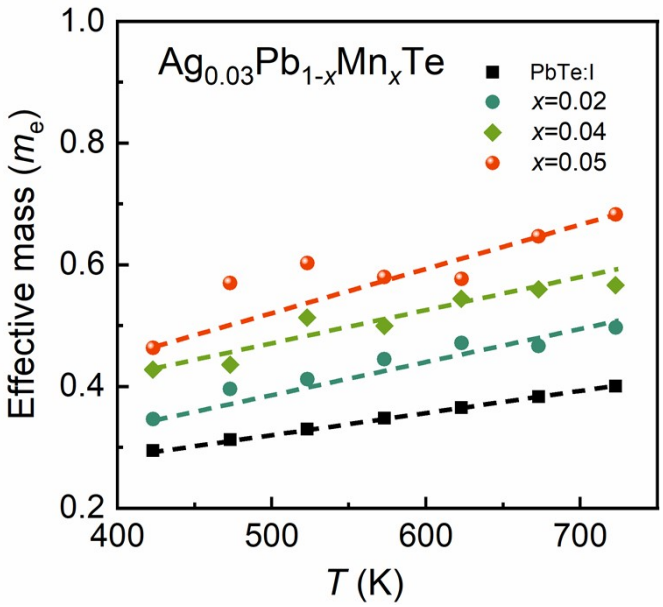

Figure S6. Temperature-dependent effective masses m^* of PbTe and $Ag_{0.03}Pb_{1-x}Mn_xTe$ (x = 0.02, 0.04, 0.05), the black scatter values are from the reported I doped PbTe material.[6]

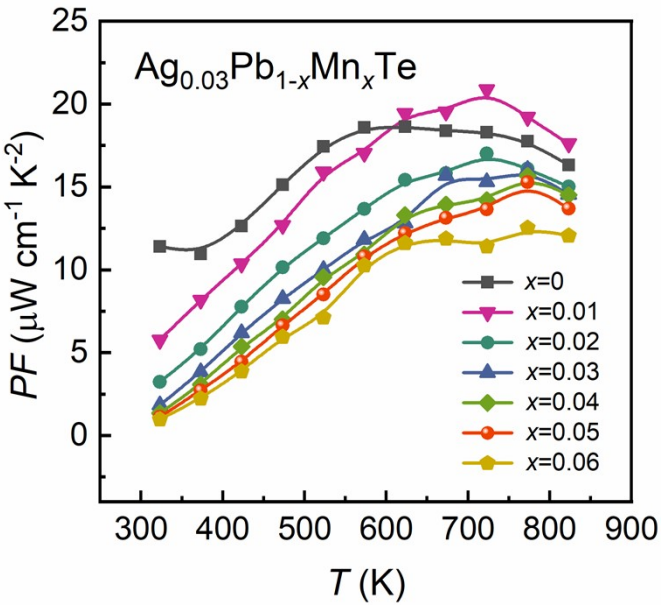

Figure S7. Temperature-dependent power factor *PF* for *n*-type $Ag_{0.03}Pb_{1-x}Mn_xTe$ samples.

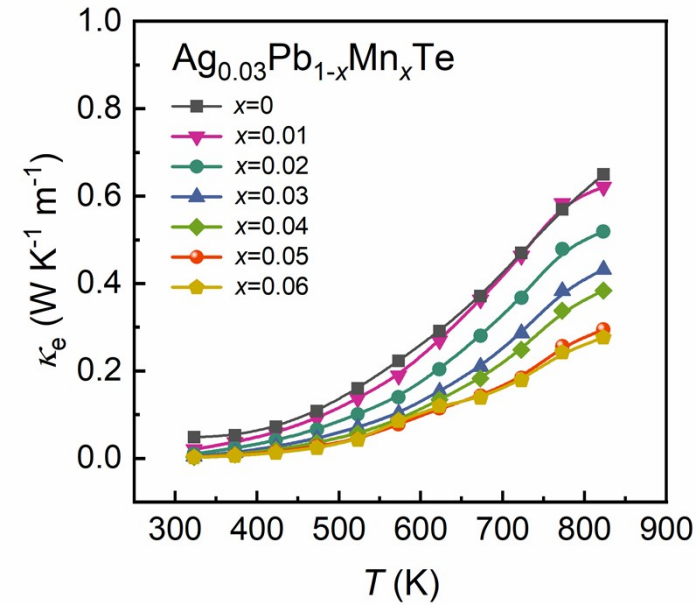

Figure S8. Temperature-dependent electrical thermal conductivity κ_e for *n*-type $Ag_{0.03}Pb_{1-x}Mn_xTe$ samples.

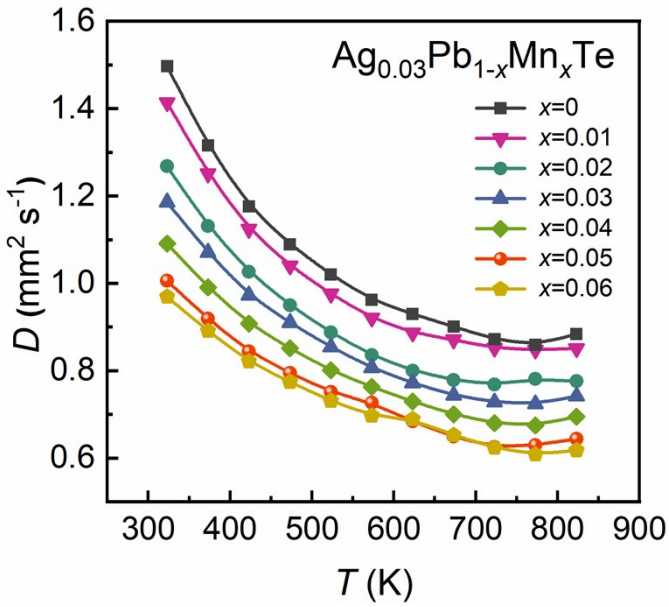

Figure S9. Temperature-dependent thermal diffusivity (D) for n-type $Ag_{0.03}Pb_{1-x}Mn_xTe$ samples.

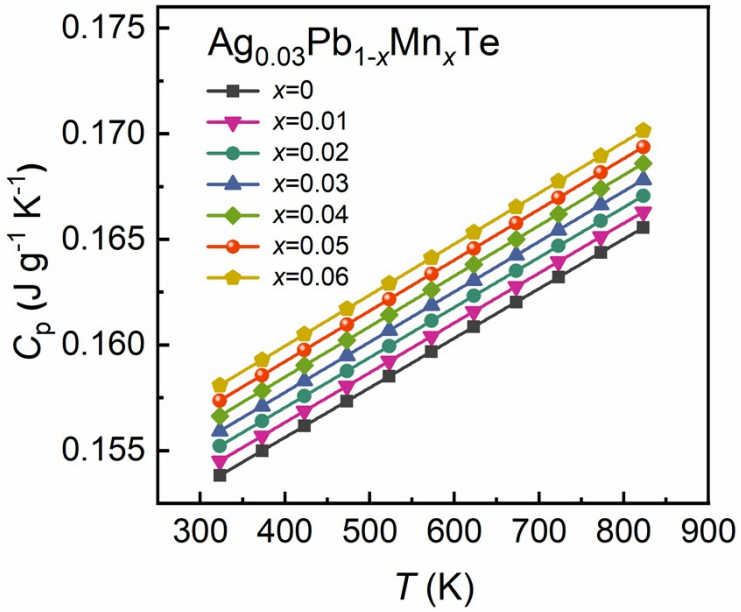

Figure S10. Temperature-dependent heat capacity (C_p) for *n*-type $Ag_{0.03}Pb_{1-x}Mn_xTe$ samples.

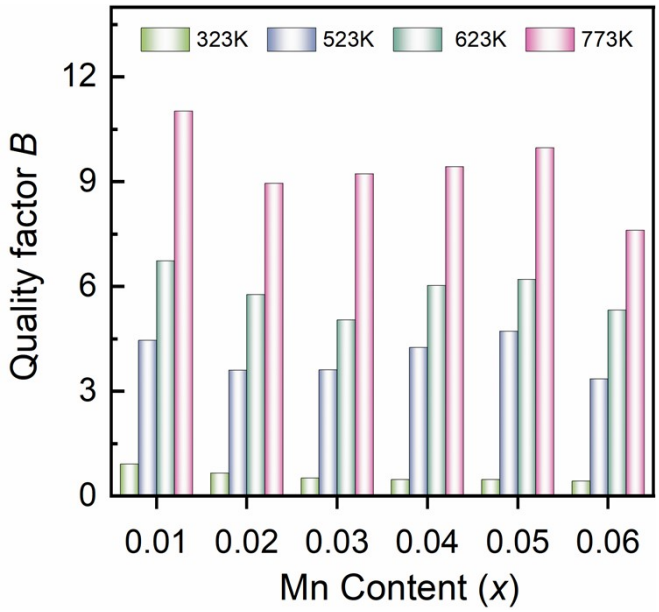

Figure S11. The calculated quality factor *B* at 323 K, 523 K, 623 K and 773 K for *n*-type $Ag_{0.03}Pb_{1-x}Mn_xTe$ samples.

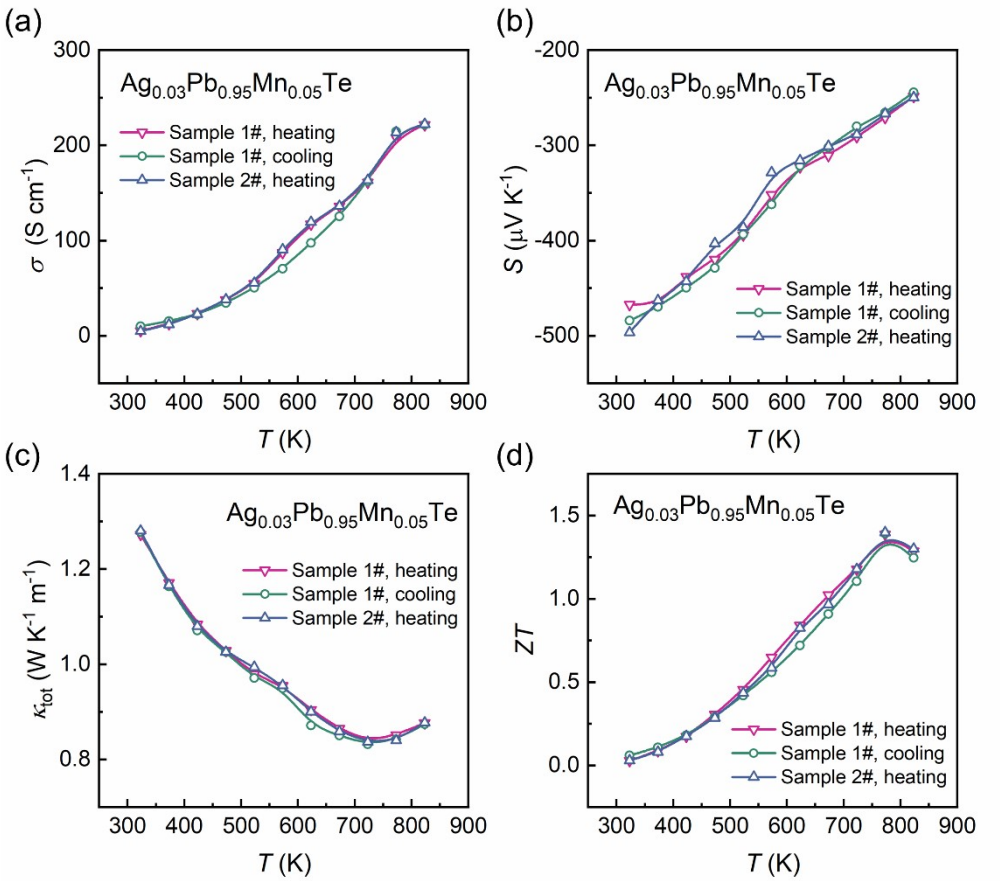

Figure S12. Thermal stability and reproducibility of (a) electrical conductivity σ; (b) Seebeck coefficient S, (c) total thermal conductivity κ_{tot}, and (d) figure of merit ZT for the high-performance n-type $Ag_{0.03}Pb_{0.95}Mn_{0.05}Te$ sample.

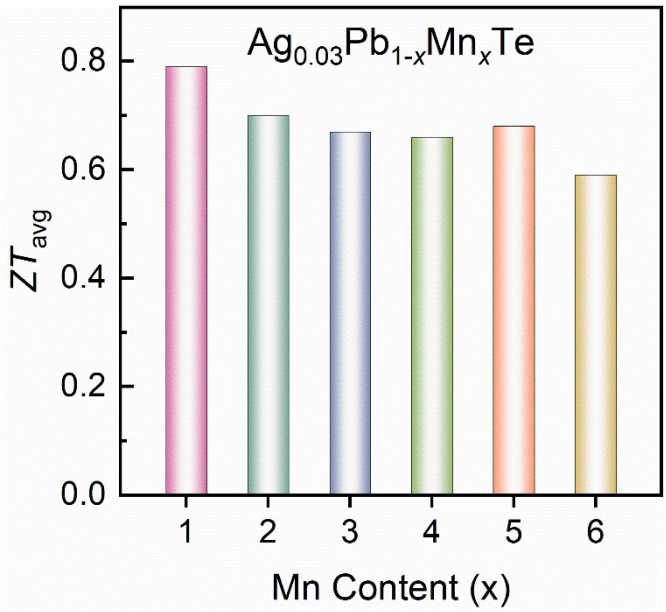

Figure S13. The average ZT (ZT_{avg}) for $Ag_{0.03}Pb_{1-x}Mn_xTe$ samples.

3. Supplementary tables

Table S1. The sample densities of $Ag_{0.03}Pb_{1-x}Mn_xTe$ (x = 0, 0.01, 0.02, 0.03, 0.04, 0.05, 0.06) measured by Archimedes method.

Sample No.	Measured density (g cm^{-3})	Relative density (%)
x=0	8.17	99.15
x=0.01	8.099	98.29
x=0.02	8.098	98.28
x=0.03	8.003	97.12
x=0.04	8.087	98.14
x=0.05	8.037	97.53
x=0.06	8.167	99.11

Table S2. The input parameters based on the theoretical simulation of lattice thermal conductivity in this work.

Parameters	Symbol	Value	Ref.
Gruneisen parameter	γ	1.65	[3]
Debye temperature	θ_D (K)	163	[17]
Average sound velocity	v (m/s)	1720	[17]
Average atomic mass for PbTe	M (kg)	2.78×10^{-25}	[18]
Ratio of N- to U- process	A_N	2.9	[19]
Phenomenological parameter		65	[18]
Mole mass of Pb	M_{Pb} (g/mol)	207.2	-
Mole mass of Te	M_{Te} (g/mol)	127.6	-
Mole mass of Ag	M_{Ag} (g/mol)	107.8682	-
Mole mass of Mn	M_{Mn} (g/mol)	54.938	-
Radius of Pb atom	r_{Pb} (Å)	1.2	-
Radius of Ag atom	r_{Ag} (Å)	1.26	-
Radius of Mn atom	r_{Mn} (Å)	0.8	-

References

1 H. J. Wu, C. Chang, D. Feng, Y. Xiao, X. Zhang, Y. L. Pei, L. Zheng, D. Wu, S. K. Gong, Y. Chen, J. Q. He, M. G. Kanatzidis and L. D. Zhao, *Energy Environ. Sci.*, 2015, **8**, 3298-3312.

2 Y. I. Ravich, B. A. Efimova and V. I. Tamarchenko, *Phys. Status Solidi B.*, 1971, **43**, 11-33.

3 Y. I. Ravich, B. A. Efimova, I. A. Smirnov and L. S. Stil'bans, *Semiconducting Lead Chalcogenides*, Plenum Press, New York, 1970.

4 R. S. Allgaier, *J. Appl. Phys.*, 1961, **32**, 2185-2189.

5 H. A. Lyden, *Phys. Rev.*, 1964, **135**, A514-A521.

6 Y. Z. Pei, A. D. LaLonde, H. Wang and G. J. Snyder, *Energy Environ. Sci.*, 2012, **5**, 7963-7969.

7 Y. I. Ravich, B. A. Efimova and V. I. Tamarchenko, *Phys. Status Solidi B.*, 1971, **43**, 453-469.

8 Y. Z. Pei, Z. M. Gibbs, A. Gloskovskii, B. Balke, W. G. Zeier and G. J. Snyder, *Adv. Energy Mater.*, 2014, **4**, 12.

9 J. Callaway and H. C. Vonbaeyer, *Phys. Rev. Lett.*, 1960, **5**, 223-223.

10 G. J. Snyder, A. H. Snyder, M. Wood, R. Gurunathan, B. H. Snyder and C. N. Niu, *Adv. Mater.*, 2020, **32**, 5.

11 Y. Z. Pei, A. F. May and G. J. Snyder, *Adv. Energy Mater.*, 2011, **1**, 291-296.

12 Q. Zhang, Q. C. Song, X. Y. Wang, J. Y. Sun, Q. Zhu, K. Dahal, X. Lin, F. Cao, J. W. Zhou, S. Chen, G. Chen, J. Mao and Z. F. Ren, *Energy Environ. Sci.*, 2018, **11**, 933-940.

13 H. T. Liu, Q. Sun, Y. Zhong, Q. Deng, L. Gan, F. L. Lv, X. L. Shi, Z. G. Chen and R. Ang, *Nano Energy*, 2022, **91**, 106706.

14 L. You, J. Y. Zhang, S. S. Pan, Y. Jiang, K. Wang, J. Yang, Y. Z. Pei, Q. Zhu, M. T. Agne, G. J. Snyder, Z. F. Ren, W. Q. Zhang and J. Luo, *Energy Environ. Sci.*, 2019, **12**, 3089-3098.

15 Y. Zhong, H. T. Liu, Q. Deng, F. L. Lv, L. Gan and R. Ang, *ACS Appl. Mater. Interfaces*, 2021, **13**, 52802-52810.

16 X. L. Su, S. Q. Hao, T. P. Bailey, S. Wang, I. Hadar, G. J. Tan, T. B. Song, Q. J. Zhang, C. Uher, C. Wolverton, X. F. Tang and M. G. Kanatzidis, *Adv. Energy Mater.*, 2018, **8**, 11.

17 Y. Xiao, H. J. Wu, J. Cui, D. Y. Wang, L. W. Fu, Y. Zhang, Y. Chen, J. Q. He, S. J. Pennycook and L. D. Zhao, *Energy Environ. Sci.*, 2018, **11**, 2486-2495.

18 Z. S. Wang, H. He, X. D. Cui, H. T. Liu, W. B. Qiu, L. Q. Chen, B. Q. Zhou, J. Tang and R. Ang, *J. Appl. Phys.*, 2019, **125**, 6.

19 L. W. Fu, M. J. Yin, D. Wu, W. Li, D. Feng, L. Huang and J. Q. He, *Energy Environ. Sci.*, 2017, **10**, 2030-2040.